Ultrathin active polarization-selective metasurface at X-band frequencies

Josip Lončar [ORCID],[1,*] Anthony Grbic,[2] and Silvio Hrabar[1]

[1]*Faculty of Electrical Engineering and Computing, University of Zagreb, Unska 3, 10000 Zagreb, Croatia*
[2]*Radiation Laboratory, Department of Electrical Engineering and Computer Science, University of Michigan,
Ann Arbor, Michigan 48109-2122, USA*

An ultrathin active polarization-selective metasurface is designed and optimized for operation in the X band. The metasurface leverages the design of a previously reported passive polarization converting metasurface. Similar to the passive polarization converter, the proposed active metasurface consists of three patterned metallic sheets. Its bottom sheet is modified and populated with ultrawideband, unconditionally stable amplifiers and corresponding biasing networks. The metasurface provides over 35 dB of input-output isolation achieved through orthogonal polarizations, which ensures stable operation. It was fabricated with a low-cost, printed-circuit-board and pick-and-place process. The performance of the metasurface was measured and its stability confirmed. The desired effects of amplification, polarization conversion, polarization selectivity, and nonreciprocal behavior were successfully demonstrated in both full-wave simulations and measurements. Due to its extremely small thickness (0.66 mm or 0.02λ at 10 GHz), the metasurface shows excellent performance for a wide range of incident angles, which exceeds $\pm 30°$. It achieves a perfect (100%) polarization conversion ratio in simulation, and 98.4% in measurement.

I. INTRODUCTION

Manipulating electromagnetic waves has always been an appealing field of science, which has led to the research and development of artificial electromagnetic structures, known as metamaterials. Over the past few years, numerous advances have been made in the area of passive metasurfaces: subwavelength-patterned metallic/dielectric two-dimensional metamaterials. Passive metasurfaces have shown great flexibility in manipulating electromagnetic waves in terms of beam forming [1], filtering [2], wavefront [3], and polarization control [3]. In polarization control, metasurfaces have shown superior performance in terms of size and efficiency over conventional methods [4–7]. Multilayer design led to further improvements in terms of power efficiency and polarization conversion ratio (*PCR*) [3,8–15]. Some reported polarization converting metasurfaces achieve *PCR*s exceeding 95% [8,9,14,15].

While passive metasurfaces have been extensively investigated, active metasurfaces have only begun to be explored. Active metasurfaces employ active electronic circuitry to provide new functionalities, such as amplification [16–18], nonreciprocal responses [16–18], dynamic reconfigurability [17,19], and dynamic tunability [20], to overcome the fundamental constraints of passive metasurfaces. Active metasurfaces that provide amplification of electromagnetic radiation are of particular interest. They face certain challenges such as instability of operation, which manifests itself as unwanted, uncontrolled oscillations. The problem of instability is especially pronounced in the radio frequency regime, where

parasitic feedback loops are difficult to estimate and control. The two main categories of active electromagnetic structures are grid amplifiers [16] and active reflectarrays [17]. Although successful efforts in the development of both structures have been reported, opportunities for further improvement still exist. For example, a grid amplifier requires additional polarizers to ensure stable operation [16], which makes the design bulky. On the other hand, a reflectarray's bandwidth is limited [17] by the weak interaction between radiating elements [21,22]. In transmission, the stability problem has been solved by introducing a ground plane between two layers of the structure, which provides isolation and prevents input-output coupling [18]. In reflection, isolation can be achieved using orthogonal polarizations for the incident and reflected waves. We propose an ultrathin, active metasurface that selectively controls the polarization of an incident wave upon reflection, with simulated *PCR* reaching 100%. The active metasurface leverages the design of a recently reported passive polarization converter [15], making it possible to overcome the above mentioned challenges, and design a highly compact, low-profile metasurface with broader bandwidth and improved performance for oblique incidence. Much like the passive metasurface, this active one consists of three patterned metallic layers, which allows efficient coupling to impinging electromagnetic radiation. Populated with active electronic circuitry, it provides amplification of the captured energy and polarization selectivity. Orthogonality of the input and output elements of the structure leads to conversion of the selected polarization. Demonstrating the effects of amplification, polarization conversion, polarization selectivity, and a nonreciprocal response, the metasurface represents an adequate compact and lightweight substitution for magnet-based nonreciprocal devices operating in reflection, such as
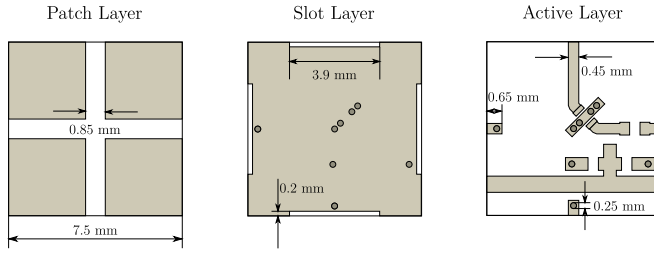
_____
*josip.loncar@fer.hr

FIG. 1. Unit cell layers of the active polarization-selective metasurface.

isolators [23]—the metasurface absorbs one orthogonal polarization of incident wave, while it amplifies and reflects the other.

II. METASURFACE DESIGN

The square unit cell of the active polarization-selective metasurface is shown in Figs. 1, 2, and 3. In Fig. 1 the layers of the proposed unit cell are depicted. The unit cell comprises three layers: a top patch layer, a middle slot layer, and a bottom active layer. Each layer represents a pattern etched in an 18 μm thick copper cladding. At the operating frequency of 10 GHz, the unit cell dimension of the active metasurface is $0.25\lambda_0$ (free space wavelengths), and its thickness is only $0.02\lambda_0$.

The size of patches on the top layer is 6.65 mm, which is $0.22\lambda_0$ or $0.42\lambda_d$ (wavelengths in the dielectric, $\epsilon_r = 3.55$). The values of all the design parameters are given in Figs. 1 and 3. Each patch is shared between four adjacent unit cells. The middle layer consists of a ground plane with slots. The slots are placed along the sides of the unit cell, and also shared between adjacent unit cells. In the design, the bottom layer, detailed in Fig. 2, is aperture coupled to a resonant tank formed by the patch array and ground plane [15,24–26].
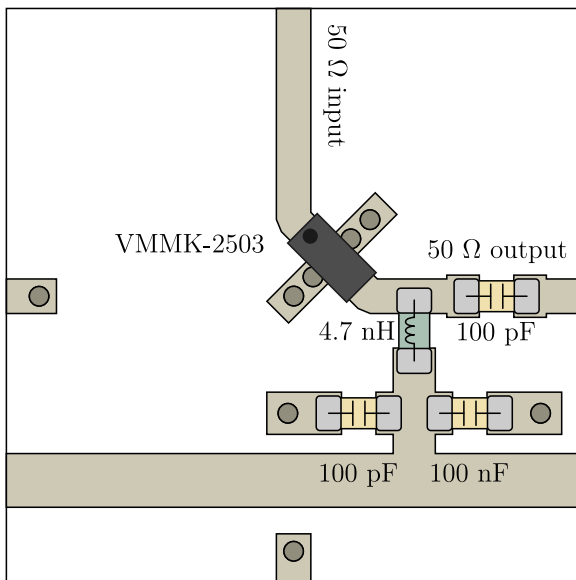

FIG. 2. Bottom layer of the active polarization-selective metasurface.
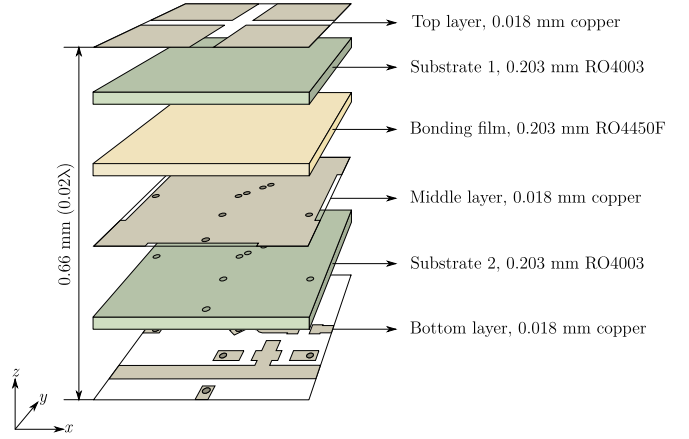

FIG. 3. A stack-up of the unit cell of the active polarization-selective metasurface.

The bottom layer contains microstrip lines terminated by vias close to the edge of unit cell. The microstrip line is split into two segments, providing space for an amplifier at the center of unit cell. Each segment extends to two adjacent cells in the x and y directions. Each cell also provides terminations (shorting vias) for segments originating in two adjacent cells. In the design, the ultrawideband, unconditionally stable amplifier VMMK-2503 by Avago Technologies was chosen. The amplifier is in E-pHEMT (enhancement mode pseudomorphic high electron mobility transistor) technology and comes in a 0402 surface mount package (1 mm × 0.5 mm). It requires relatively high DC power (65 mA at 5 V, or 325 mW) for optimal performance, and provides a small-signal gain of 13.5 dB. The input and the output impedance of the amplifier is 50 Ω. To minimize reflection, the microstrip line is designed to have a characteristic impedance equal to 50 Ω. Thus, no matching network is needed. The vertical segment of the microstrip line shown in Fig. 2 represents the input, while the horizontal segment represents the output. A simple biasing network, consisting of a parallel combination of two capacitors (100 pF and 100 nF) and an inductor (4.7 nH), was placed close to the output terminal of the amplifier. The biasing network provides the DC voltage and current needed for setting the operating point of the amplifier, while preventing high frequency signals from entering the horizontal DC biasing line [27]. Each row of unit cells is powered by the same DC biasing line. An additional 100 pF capacitor is incorporated into the output microstrip line segment as a DC block. The input of the amplifier is AC coupled, thus no DC-blocking capacitor is needed. All capacitors and inductors were in 0402 surface mount packages. The orthogonal orientation of the input and output microstrip segments is crucial for stable operation of the active metasurface. It reduces feedback: coupling between the amplifier's input and output.

Common configurations of dual-polarized orthogonal aperture-coupled patches can be found in literature [28,29]. In the proposed design, however, the orthogonal excitation of the structure is achieved by the shared elements of adjacent unit cells, as explained above (for additional information, refer to Sec. II of [15]). The sharing occurs at each layer of the metasurface. A stack-up of the printed circuit board is shown in Fig. 3. Three 18 μm thick copper layers are separated

by two 0.203 mm thick RO4003 substrates ($\epsilon_r = 3.55$). The substrates with patterned copper cladding are bonded together using 0.203 mm thick RO4450F ($\epsilon_r = 3.52$) bonding film. The middle and the bottom copper layers are electrically connected through substrate 2 using two blind vias per cell that terminate the input and output microstrip lines of the amplifier.

### III. POLARIZATION SELECTIVITY AND NONRECIPROCAL RESPONSE

Let us assume that an incident electromagnetic wave, polarized in the y direction, impinges onto the periodic structure with the unit cell shown in Fig. 3 in the negative z direction. The incident wave induces an electric field across the x-directed gaps between patches. The electromagnetic energy is captured by the resonant tank formed by the patch array and ground plane. Since the incident electromagnetic wave is polarized in y direction, it is coupled to the y-directed 50 Ω microstrip lines on the bottom layer through the x-directed slots in the ground plane. This coupling mechanism is equivalent to the coupling mechanism of the passive polarization converting metasurface (see Sec. II of [15]). The microstrip lines guide the energy to the amplifiers' input. Due to impedance matching between the amplifiers' input impedance and the characteristic impedance of the microstrip lines, there is very little reflection. This significantly reduces copolarized reflection from the metasurface. The signal amplified by the amplifiers is guided by the x-directed segments of the microstrip lines to the y-directed slots in the ground plane. Since the input and output slots are orthogonal to each other, the electric field is converted to an orthogonal polarization. Each segment of microstrip lines is terminated with a blind via, which ensures maximum magnetic field at the slot position, and results in broadband magnetic field coupling. Apart from energy coupling, the slots enable impedance matching between free space ($\eta_0 = 376.73 \ \Omega$) and the microstrip lines ($Z_0 = 50 \ \Omega$) achieved through an optimization of the slot geometry for minimal copolarized reflections using the commercial electromagnetic solver Ansys HFSS. Once the energy reaches the y-directed slots at the output, it is coupled back to the resonant tank. As a result, an electric field is excited across the y-directed gaps between the patches, and the wave is radiated back polarized in the x (orthogonal) direction.

If the metasurface is illuminated with an x-polarized electromagnetic wave, the wave is coupled to the x-directed segments of the microstrip lines through y-directed slots, and guided to the amplifiers' output. Here most of the energy is absorbed by the amplifiers. Only a small portion is reflected due to imperfect matching between the amplifiers' output impedance and the characteristic impedance of the microstrip lines, causing copolarized reflection from the metasurface. Since amplifiers are not perfectly unilateral ($|s_{12}| \neq 0$), a small portion of incident energy is transferred to the input ports of the amplifiers, which contributes to cross-polarized reflection from the metasurface. However, both copolarized and cross-polarized reflected waves are highly attenuated.
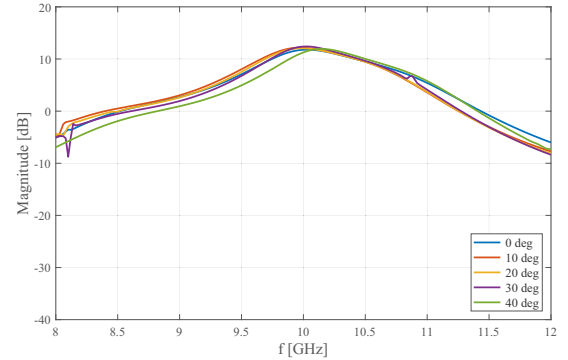
For an arbitrarily polarized incident wave, the metasurface amplifies the y-polarized component of the electric field and radiates it back orthogonally polarized, while absorbing
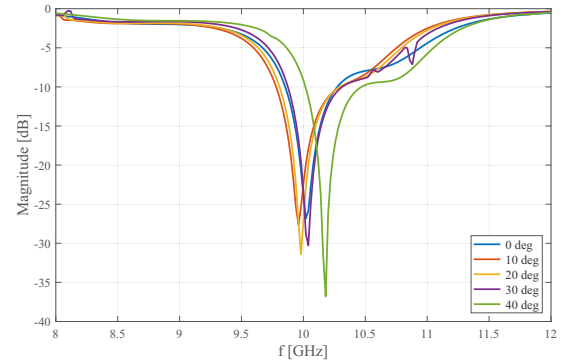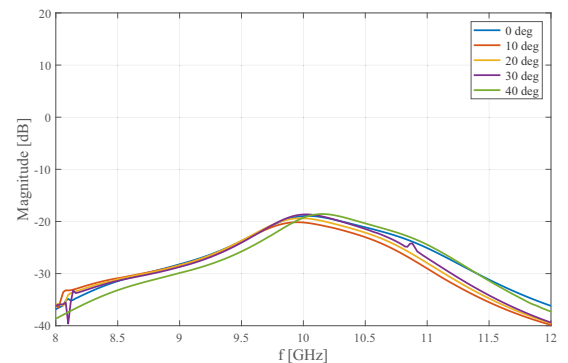

(a) Cross-polarized reflection, R_{xx}.
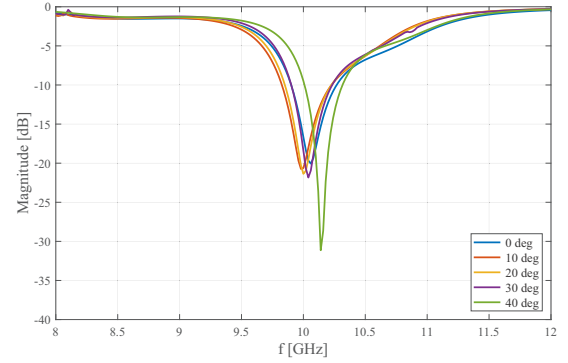
(b) Co-polarized reflection, R_{yy}.

(c) Cross-polarized reflection, R_{xy}.

(d) Cross-polarized reflection, R_{yx}.

FIG. 4. Simulated reflection coefficients of the proposed metasurface for different incident angles.

the x-polarized component of the incident electric field. Thus, the metasurface is truly polarization selective. The polarization selectivity is entirely due to the nonreciprocal behavior of the amplifiers. Reflection coefficients of the
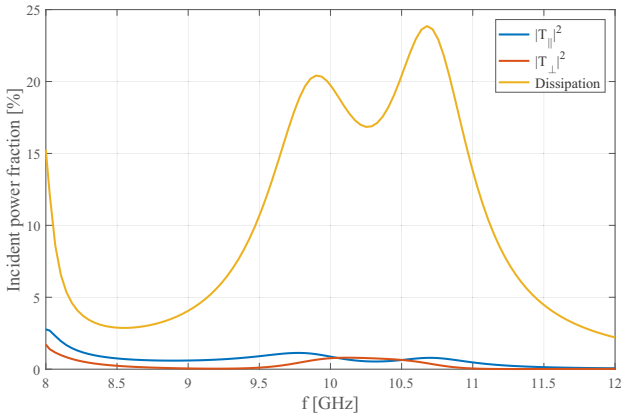
FIG. 5. Simulated contribution of the loss mechanisms in the active polarization-selective metasurface.

proposed active polarization-selective metasurface for different incident angles are shown in Fig. 4. They are obtained from simulations of the amplifier's scattering parameters (S-parameters) in Keysight ADS combined with S-parameters of the passive parts of the structure obtained from simulations in Ansys HFSS. See Supplemental Material [30] for a detailed description of both models. The metasurface is well matched to free space for both x-polarized ($|R_{xx}| < -10$ dB) and y-polarized ($|R_{yy}| < -10$ dB) incident waves. A small cross-polarized reflection coefficient $|R_{yx}| < -10$ dB indicates strong absorption of an x-polarized incident wave, while a high cross-polarized reflection coefficient $|R_{xy}| > 0$ dB indicates amplification and polarization conversion of a y-polarized incident wave, with a peak value of 11.3 dB. The amplification occurs in the frequency range from 9.65 to 11.25 GHz. The difference between the cross-polarized reflection coefficients is a clear indication of the nonreciprocal response ($R_{xy} \neq R_{yx}$). The metasurface is optimized for normal incidence, so the performance is expected to degrade with increasing angle of incidence. However, Fig. 4 indicates that it performs quite well for a wide range of incident angles exceeding $\pm 30°$.

There are two main loss mechanisms present in the proposed active, polarization-selective metasurface. Loss occurs either due to unwanted transmission through the structure (leakage), or dissipation in the materials. The relative contribution of the loss mechanism in the X band is shown in Fig. 5. Only a small fraction of incident power (less than 2%) can be attributed to copolarized and cross-polarized transmission. At the central frequency, around 20% of incident power is dissipated due to the finite conductivity of copper and substrate loss. The losses within the metasurface were investigated in simulation only, due to practical limitations of the measurement setup and available equipment, which does not allow measurement of transmitted power without disrupting system calibration.

IV. STABILITY CONSIDERATIONS

A major challenge with all active electromagnetic structures incorporating amplifiers is instability. Instability can occur due to the unintentional positive feedback of an unconditionally stable amplifier through the passive parts of
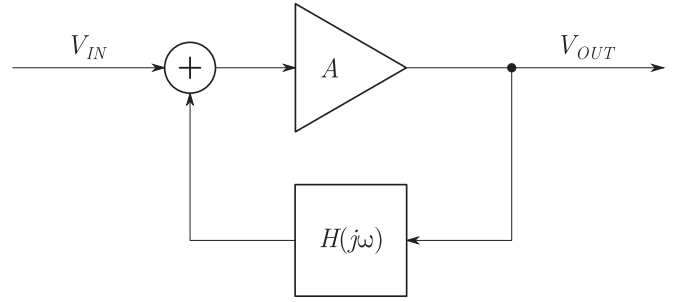

FIG. 6. Simplified model of an amplifier and its passive environment.

the metasurface. Not only are the parasitics through which the feedback occurs unavoidable at X-band frequencies, but they are also very difficult to estimate. The parasitic feedback loop is represented by the transfer function $H(j\omega)$ in Fig. 6. Here A represents the amplifier's gain. If the Barkhausen stability criterion $AH(j\omega) = 1$ [23] is satisfied, an output voltage $V_{OUT} \neq 0$ may exist, even though the input voltage $V_{IN} = 0$. Since the VMMK-2503 amplifier provides a small-signal gain of 13.5 dB, Barkhausen criterion is satisfied if $H(j\omega) = -13.5$ dB. The instability manifests itself as oscillations at the frequency ω at which the criterion is satisfied. This analysis does not take into account imperfections present in the amplifiers (e.g., limited bandwidth, finite input impedance, finite slew rate, delay, etc.), which may cause differences between calculated and actual instability conditions. However, to ensure stable operation of the metasurface, it is sufficient to ensure the amplifier input-output isolation remains higher than the predicted margin of 13.5 dB. The amplifier input-output coupling, shown in Fig. 7, is significantly reduced due to the orthogonally oriented input and output microstrip lines and slots in the ground plane. An input-output isolation of more than 25 dB in the frequency range from 0.5 to 20 GHz, and more than 35 dB in the X band ensured stable operation of the metasurface.

V. EXPERIMENTAL VERIFICATION

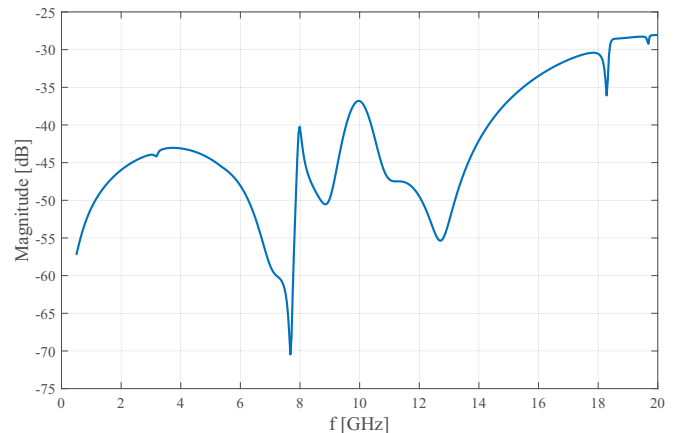The active polarization-selective metasurface was fabricated using a standard printed-circuit-board process and
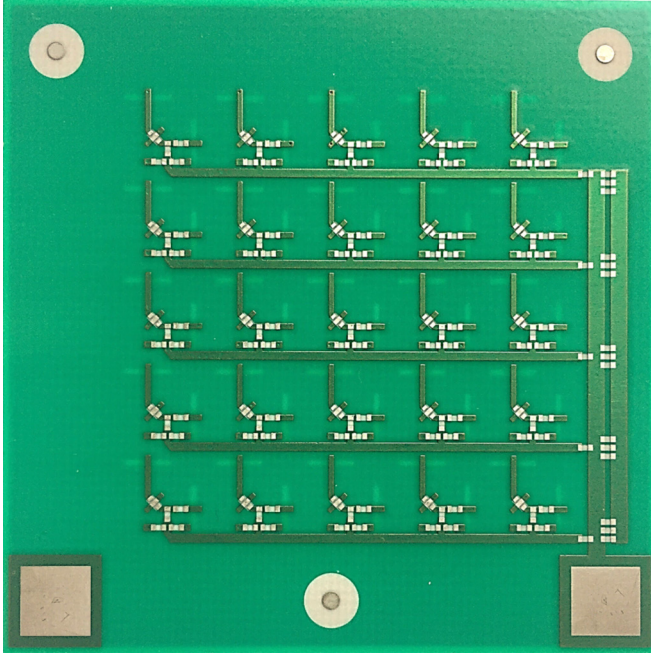

FIG. 7. Simulated amplifiers' input-output coupling.

FIG. 8. Bottom layer of the fabricated active polarization-selective metasurface.

FIG. 9. Schematic of the quasioptical, free-space measurement setup [15,31–33].

assembled using surface mount technology (SMT) component placement system (pick-and-place machine). The board consisted of an array of 5 × 5 active unit cells, which occupied an area of 37.5 × 37.5 mm^2 (1.25λ × 1.25λ). The overall board size was 53.9 × 53.9 mm^2 (1.8λ × 1.8λ) with a thickness of approximately 0.66 mm (0.02λ). Figure 8 shows a bottom view of the fabricated metasurface. Each row of unit cells is biased by the same line. The length of the biasing lines is limited only by the number of amplifiers. If there are too many, the DC biasing current may cause a voltage drop along the biasing line, which can cause differences in operating point between amplifiers in the same row. Moreover, too many amplifiers in such a dense arrangement may cause overheating problems. At the end of each row an additional biasing network, equivalent to one used in each unit cell, was added, which improved the RF isolation between the rows. The metasurface was powered using two pads placed at the bottom left and right corners. The left power pad was connected to the ground plane using nine blind vias.

To measure the S-parameters of the fabricated device in free space, the board was illuminated with a Gaussian beam. In order to produce a collimated beam confined to a small radius, quasioptical Gaussian beam telescopes were used [31–33]. Each telescopic system consisted of a dual-polarized rectangular horn antenna and a pair of lenses made of Rexolite (n = 1.59). The diameters of the lenses were 32.5 cm, with input and output focal lengths of 45 cm. The telescopic systems were placed on two linear translation stages, whose position was controlled by stepper motors with a 5 μm accuracy. The vertical and horizontal feeds of the antennas were connected to the ports of an Agilent E8361A vector network analyzer (VNA) used for measurement of the S-parameters for both polarizations. The measurement setup is shown in Fig. 9. Before measurement, the system
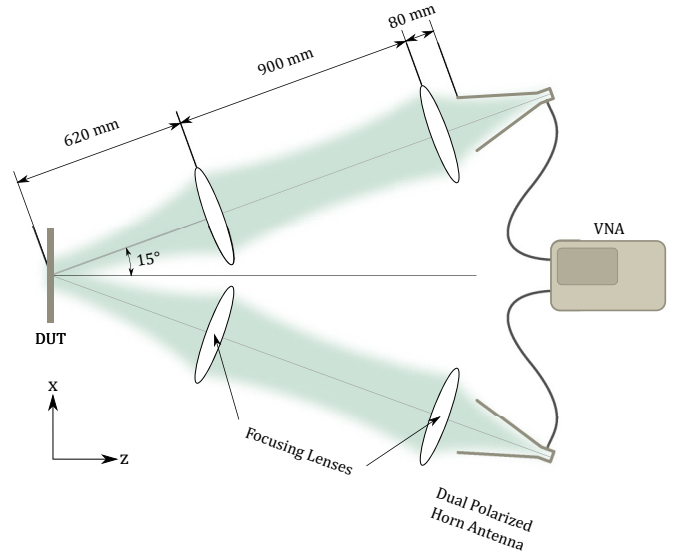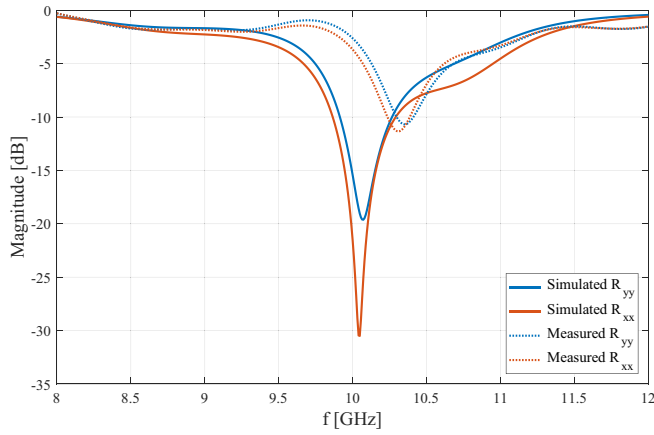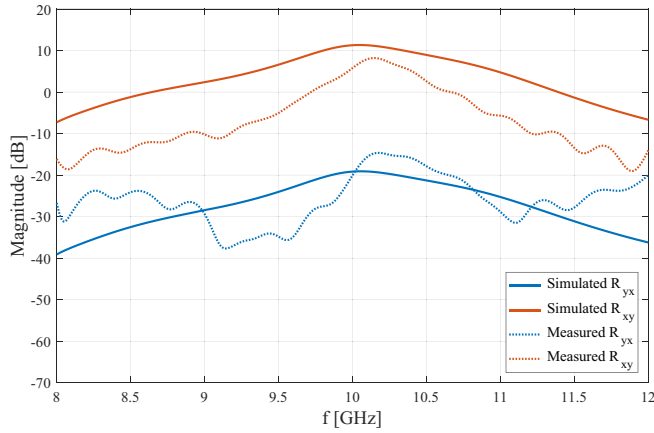
was calibrated using the TRL (thru, reflect, line) calibration method [34]. Polarization converters are challenging to characterize for normal incidence. The problem lies in the fact that an ideal polarization rotator needs to be used as a thru standard for proper calibration. Thus, the performance of proposed active polarization-selective metasurface was measured for an oblique incidence at 15° with respect to normal, as shown in Fig. 9. Time gating was applied to eliminate unwanted reflection that occurs between the pairs of lenses. Figure 10 shows the magnitude of the copolarized and cross-polarized reflected wave obtained from measurement and full-wave simulation for oblique incidence at 15° angle of incidence. The measurement confirmed stable operation of the fabricated active metasurface. A small 3% frequency shift toward higher frequencies can be attributed to fabrication tolerances. The measured copolarized reflection is low for both x-polarized and y-polarized incident waves. When illuminated with a wave polarized in the y direction, the metasurface reflects an amplified, cross-polarized wave ($|R_{xy}| > 0$ dB). If illuminated with a wave polarized in x direction, the metasurface absorbs the wave ($|R_{yx}| << 0$ dB). The difference in cross-polarized reflection coefficients ($|R_{xy}| \neq |R_{yx}|$) indicates a nonreciprocal response for the metasurface. The evident discrepancy between the measurement and full-wave simulation is attributed to the small size of active area and truncation effects, which led to diffraction from the device and an imperfect calibration. Increasing the size of the structure solves this problem. However, it increases the cost of fabrication of the metasurface.

In reflection, the figure of merit for a polarization converting devices is the *PCR*. It is defined as the ratio of reflected cross-polarized power to overall reflected power. It is calculated as [9,35,36]

$$PCR = \frac{P_{R\perp}}{P_{R\perp} + P_{R\parallel}} = \frac{|R_\perp|^2}{|R_\perp|^2 + |R_\parallel|^2}. \tag{1}$$

(a) Co-polarized reflection, $R_{||}$.

(b) Cross-polarized reflection, $R_{\perp}$.

FIG. 10. Comparison between the simulated and measured reflection coefficients for a 15° angle of incidence.
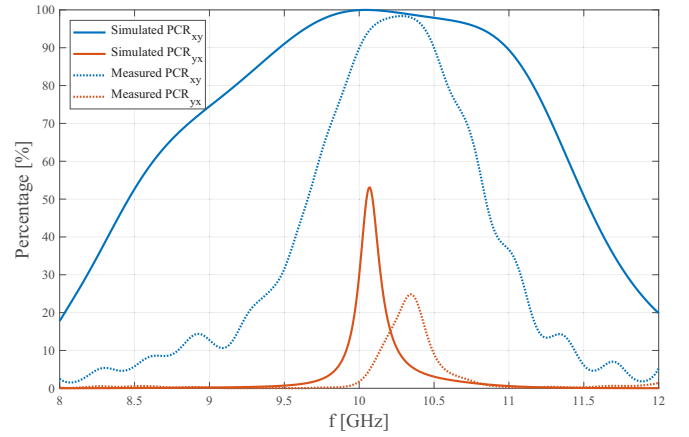

FIG. 11. Polarization conversion ratio of the active polarization-selective metasurface.

VI. CONCLUSION

In this paper an ultrathin active, polarization-selective metasurface was presented. The metasurface selectively amplifies an incident y-polarized wave, converts its polarization, and reflects it to an orthogonal polarization with perfect 100% *PCR* in simulation, and 98.4% in measurement. Due to its nonreciprocal behavior, an x-polarized incident wave is absorbed. The polarization selectivity of the metasurface stems from the nonreciprocal response of the amplifiers integrated into the metasurface design. Stable operation of the amplifiers is ensured through careful design, and the minimization of input-output coupling through the structure. The metasurface provides over 35 dB of input-output isolation at X-band frequencies. Due to its extremely small thickness (0.66 mm or 0.02λ at 10 GHz), the metasurface shows excellent performance over a wide range of incident angles, which exceeds ±30°. The performance of the fabricated metasurface was measured and its stability confirmed. Despite the differences between measurement and full-wave simulation caused by the truncation effects and challenging calibration procedure, all the desired effects were successfully demonstrated: amplification, polarization conversion, polarization selectivity, and nonreciprocal behavior. The proposed metasurface may serve as a lightweight and compact substitution for conventional nonreciprocal devices such as isolators. Moreover, by varying the length of microstrip lines in the bottom layer it is possible to create phase gradients, which would control the reflected wave angle. Furthermore, incorporation of phase shifters could lead to dynamic control and steering of reflected electromagnetic radiation. However, it is still unclear whether sufficient isolation and stable operation can be achieved without polarization conversion of an incident wave. This will be the subject of the future research efforts.

Here $R_{\perp}$ and $R_{||}$ represent cross-polarized and copolarized reflection coefficients, respectively. The squared values of each term relate incident power to cross-polarized and copolarized power. Thus, the lower the copolarized power (i.e., $|R_{||}|^2$), the higher the *PCR*. In practice, copolarized power and losses always exist, which reduce the *PCR*. To compensate, the cross-polarized power is amplified:

$$PCR = \frac{A|R_{0\perp}|^2}{A|R_{0\perp}|^2 + |R_{||}|^2}. \tag{2}$$

Here A represents the amplifier's power gain, while $|R_{0\perp}|^2$ relates incident to cross-polarized power in the case of unit power gain ($A = 1$). If $A \rightarrow \infty$, $PCR \rightarrow 100\%$. Due to the nonreciprocal response of the metasurface, two *PCR*s are defined: PCR_{xy} for a y-polarized incident wave, and PCR_{yx} for an x-polarized incident wave. They are shown in Fig. 11. The metasurface performs extremely well in converting a y-polarized incident wave, with the simulated PCR_{xy} reaching 100%, and measured PCR_{xy} of 98.4%. Recall that the metasurface absorbs an x-polarized incident wave. Thus, only a small fraction of the incident power is reflected as cross-polarized radiation, which results in a low PCR_{yx}.

[1] B. B. Tierney, Ph.D. thesis, The University of Michigan, 2016.
[2] K. Sarabandi and N. Behdad, IEEE Trans. Antennas Propag. **55**, 1239 (2007).
[3] C. Pfeiffer and A. Grbic, IEEE Trans. Microwave Theory Tech. **61**, 4407 (2013).
[4] D. Lerner, IEEE Trans. Antennas Propag. **13**, 3 (1965).
[5] L. Young, L. Robinson, and C. Hacking, IEEE Trans. Antennas Propag. **21**, 376 (1973).
[6] R.-S. Chu and K.-M. Lee, IEEE Trans. Antennas Propag. **35**, 652 (1987).
[7] M.-A. Joyal and J.-J. Laurin, IEEE Trans. Antennas Propag. **60**, 3007 (2012).
[8] P. Bouchon, Q. Lévesque, M. Makhsiyan, F. Pardo, J. Jaeck, R. Haïdar, and J.-L. Pelouard, Proc. SPIE **9371**, 93710O (2015).
[9] J. Ding, B. Arigong, H. Ren, M. Zhou, J. Shao, Y. Lin, and H. Zhang, Opt. Express **22**, 29143 (2014).
[10] L. Zhang, P. Zhou, H. Chen, H. Lu, H. Xie, L. Zhang, E. Li, J. Xie, and L. Deng, Sci. Rep. **6**, 33826 (2016).
[11] L. Cong, W. Cao, Z. Tian, J. Gu, J. Han, and W. Zhang, New J. Phys. **14**, 115013 (2012).
[12] C. Pfeiffer and A. Grbic, Appl. Phys. Lett. **102**, 231116 (2013).
[13] S.-C. Jiang, X. Xiong, Y.-S. Hu, Y.-H. Hu, G.-B. Ma, R.-W. Peng, C. Sun, and M. Wang, Phys. Rev. X **4**, 021026 (2014).
[14] G. Dong, H. Shi, S. Xia, A. Zhang, Z. Xu, and X. Wei, Opt. Commun. **365**, 108 (2016).
[15] J. Lončar, A. Grbic, and S. Hrabar, IEEE Trans. Antennas Propag. **66**, 3213 (2018).
[16] M. Kim, J. J. Rosenberg, R. P. Smith, R. M. Weikle, J. B. Hacker, M. P. De Lisio, D. B. Rutledge *et al.*, IEEE Microwave Guided Wave Lett. **1**, 322 (1991).
[17] K. K. Kishor and S. V. Hum, IEEE Trans. Antennas Propag. **60**, 197 (2012).
[18] S. Taravati, B. A. Khan, S. Gupta, K. Achouri, and C. Caloz, IEEE Trans. Antennas Propag. **65**, 3589 (2017).
[19] B. Ratni, A. de Lustrac, G.-P. Piau, and S. N. Burokur, Appl. Phys. A **124**, 104 (2018).
[20] D. F. Sievenpiper, J. H. Schaffner, H. J. Song, R. Y. Loo, and G. Tangonan, IEEE Trans. Antennas Propag. **51**, 2713 (2003).
[21] D. Pozar, Electron. Lett. **43**, 148 (2007).
[22] D. Pozar, Electron. Lett. **39**, 1490 (2003).
[23] D. M. Pozar, *Microwave Engineering* (John Wiley & Sons, New York, 2009).
[24] D. Sievenpiper, L. Zhang, R. F. J. Broas, N. G. Alexopolous, and E. Yablonovitch, IEEE Trans. Microwave Theory Tech. **47**, 2059 (1999).
[25] D. Sievenpiper, L. Zhang, and E. Yablonovitch, *1999 IEEE MTT-S International Microwave Symposium Digest (Cat. No. 99CH36282), 13-19 June 1999, Anaheim, CA, USA*, Vol. 4 (IEEE, 1999), pp. 1529–1532.
[26] G. Goussetis, A. P. Feresidis, and J. C. Vardaxoglou, IEEE Trans. Antennas Propag. **54**, 82 (2006).
[27] S. C. Cripps, *RF Power Amplifiers for Wireless Communications* (Artech House, Norwood, MA, 2006).
[28] D. M. Pozar, Electron. Lett. **21**, 49 (1985).
[29] R. Caso, A. Serra, A. Buffi, M. Rodriguez-Pino, P. Nepa, and G. Manara, IET Microwaves, Antennas & Propagation **5**, 605 (2011).
[30] See Supplemental Material at http://link.aps.org/supplemental/10.1103/PhysRevB.100.075131 for a detailed description of the full-wave model and the circuit model of the active polarization-selective metasurface.
[31] P. F. Goldsmith, Proc. IEEE **80**, 1729 (1992).
[32] S. M. Rudolph, C. Pfeiffer, and A. Grbic, IEEE Trans. Antennas Propag. **59**, 2989 (2011).
[33] S. M. Rudolph, Ph.D. thesis, The University of Michigan, 2011.
[34] Keysight Technologies, "TRL Calibration", available: http://na.support.keysight.com/pna/help/latest/S3_Cals/TRL_Calibration.htm [Online] (2018, February 20).
[35] Z. Li, S. Chen, W. Liu, H. Cheng, Z. Liu, J. Li, P. Yu, B. Xie, and J. Tian, Plasmonics **10**, 1703 (2015).
[36] W. Liu, S. Chen, Z. Li, H. Cheng, P. Yu, J. Li, and J. Tian, Opt. Lett. **40**, 3185 (2015).